Liquid Crystals
Publication details, including instructions for authors and subscription information:
http://www.tandfonline.com/loi/tlct20

Cholesterol-based dimeric liquid crystals: synthesis, mesomorphic behaviour of frustrated phases and DFT study

Dipika Debnath Sarkar [a], Rahul Deb [a], Nirmalangshu Chakraborty [a], Golam Mohiuddin [a], Rahul Kanti Nath [a] & V.S. Rao Nandiraju [a]

[a] Chemistry Department, Assam University, Silchar, India

Version of record first published: 07 Jan 2013.

To cite this article: Dipika Debnath Sarkar , Rahul Deb , Nirmalangshu Chakraborty , Golam Mohiuddin , Rahul Kanti Nath & V.S. Rao Nandiraju (2013): Cholesterol-based dimeric liquid crystals: synthesis, mesomorphic behaviour of frustrated phases and DFT study, Liquid Crystals, DOI:10.1080/02678292.2012.757814

To link to this article: http://dx.doi.org/10.1080/02678292.2012.757814

Liquid Crystals, 2013
http://dx.doi.org/10.1080/02678292.2012.757814

Taylor & Francis
Taylor & Francis Group

Cholesterol-based dimeric liquid crystals: synthesis, mesomorphic behaviour of frustrated phases and DFT study

Dipika Debnath Sarkar, Rahul Deb, Nirmalangshu Chakraborty, Golam Mohiuddin, Rahul Kanti Nath and V.S. Rao Nandiraju*

Chemistry Department, Assam University, Silchar, India

(*Received 16 October 2012; final version received 9 December 2012*)

Chiral unsymmetrical dimeric liquid crystals consisting of a cholesterol moiety as chiral entity and a substituted salicylidene imine core (with the substituent being butyl or fluoro or chloro group) interconnected through an even methylene spacer have been synthesised and their mesomorphic properties are characterised. All the dimers exhibit enantiotropic mesophases. The butyl homologue exhibited N* phase only, the fluoro- and chloro-substituted compound exhibited frustrated blue phases (BPs), N* phase and SmC* or twisted grain boundary (TGB) phases. The occurrence of a fluid frustrated phase, the BP, in particular, observed in compounds with a polar moiety and bent optimised conformation by density functional theory (DFT) study, indicates the importance of polar structures and bent shape of the compounds. Theoretical calculation was performed in order to study the optimised conformation, polarity and electron density distribution of the synthesised cholesterol derivatives using DFT. Time-dependent density functional theory (TD-DFT) calculation also had been carried out to investigate the absorption spectra and HOMO–LUMO energies. The experimental and theoretical absorption spectra are also presented.

Keywords: cholesterol; blue phase; TGB phase; frustrated phase; DFT study

1. Introduction

Since the discovery of the fourth state of matter, namely mesomorphic phase of self-organising helical superstructures in cholesteryl benzoate [1,2] chirality in ordered fluids has become one of the most fascinating field of current research in liquid crystals to develop devices such as fast-response display and tunable photonic crystals and laser emitting devices [3,4].

Two kinds of frustrated mesomorphic phases, that is, the blue phases (BPs) and the twisted grain boundary (TGB) phases are generated from helical superstructures. BPs with a lattice of defects made up of double-twist cylinders [5–15], which are normally observed as thermodynamically stable mesophases over a narrow temperature range between the isotropic (Iso) and chiral nematic (N*) phases [16,17] and TGB phases manifested by incompatible helical-lamellar smectic structures [2,18–22], have been of great interest in chiral liquid crystal systems in the last two decades. Three types of BPs are known: body-centred cubic (BPI), a simple cubic (BPII) and amorphous phases (BPIII) [23–27]. BPs have been observed only in chiral liquid crystal systems. Chirality can be introduced by the following ways: direct incorporation of chiral centres through synthetic efforts, addition of chiral dopants in achiral LC hosts and through intermolecular hydrogen bonds [28]. Extensive efforts to realise these frustrated phases revealed the importance of large helical twisting power (high chirality), optical purity of the molecules and molecular interactions based on compatibility between different segments of the molecules. Excellent reviews on dimers and higher oligomers appeared recently discussing the molecular structure–liquid crystalline property relationship [29,30]. Unsymmetrical dimesogenic compounds [31–38] consisting of cholesteryl ester unit as a chiral moiety covalently bonded to different promesogenic units, namely Schiff base, azobenzene, stilbene, ester, biphenyl fragments or functional moieties, and so on, through a polymethylene unit have been extensively studied due to their importance in basic research of structure–property relationship as well as in device applications. Hardouin et al. reported [39–42] the uncommon incommensurate fluid smectic phases and short thermal range TGB, N* and BPs in nonconventional mesogens formed by cholesterol and Schiff base linked by an alkanoic acid spacer (KI-4, KI-5]. Dimesogenic compounds based on cholesterol and *N*-(*n*-alkyl) salicylideneimines separated by a flexible spacer of varying length of *n*-alkanoicacid ($-(CH_2)_nCOO-$; $n = 3$, 4, 5 and 7) [43], the homologues with an odd parity spacer were found to exhibit SmC*–SmA*–TGB-N* phase variant in cooling cycle, while the even parity homologue ($n = 4$) exhibited only monotropic N* phase. The

*Corresponding author. Email: nandirajuv@gmail.com

lanthanide complexes exhibited only SmA* phase. The complexes of the dimesogenic compounds with an even parity methylene spacer ($n = 4$) were found to be crystalline in nature and the crystalline behaviour had been attributed to the pronounced bent molecular conformation of the constituent compounds [43,44]. The metal (Cu(II) or Pd(II)) complexes [44] of the above compounds are found to exhibit monotropic N* or SmA* phase. However, with a spacer ($n = 5$) and replacing the *N*-alkyl moiety by *N*-aryl moiety, the compound KI-5(OH) [45] exhibited N*-TGB (transient)–SmA* phase variant, while its complexes exhibited only SmA phase. Further, the occurrence of fluid frustrated phase, in particular, the BP reflecting the ultra short pitch with highly twisted conformation in dimesogens with a bent chalcone moiety at one end, is attributed due to bent–core chalcone entity in the dimer structure [13].

Hence, we are particularly interested in investigating the influence of polar substituent as well as non-polar butyl group on the possible existence of blue and TGB phases in these dimesogenic compounds synthesised using cholesterol and *N*-(4-substituted) salicylideneimines separated by a flexible even parity methylene spacer of fixed length. Here we report the synthesis and characterisation of unsymmetrical dimesogens **1-Bu**, **1-F** and **1-Cl** consisting of a cholesteryl ester and a promesogenic Schiff's base moiety with different substituents, (butyl, fluoro and chloro groups) separated by an even parity alkylene central spacer. A comparison of the mesomorphism with similar molecular structures reported earlier shall also be presented. Quantum chemical calculations based on density functional theory (DFT) study has been performed to give more insight into the molecular conformation, isoelectron density surface with electrostatic potential distribution and static polarisability. An accurate HOMO and LUMO description, namely atomic orbital composition, absolute energy and relative energy gap, provides the important information related to photo-physical properties which helps for the design of new molecules and their tuning of distinct desired properties of the compounds.

2. Experimental

All the chemicals are procured from M/S Aldrich chemicals, Alfa Aesar, Tokyo Kasei Co. Ltd., Combi Blocks. The solvents and reagents are of AR grade, and were distilled and dried prior to use. The ^{1}H nuclear magnetic resonance spectra were recorded either on JEOL FX-90Q (500 MHz) multinuclear spectrometer (chemical shift in δ) solution with TMS as internal standard. Microanalysis of C, H and N elements were determined on a Carlo-Erba 1106 elemental analyser. IR spectra were recorded on a Shimadzu IR Prestige-21, (ν_{max} in cm^{-1}) on KBr disks. A differential scanning calorimeter (DSC) (Perkin-Elmer DSC Pyris1 system) using indium as standard was used to measure the phase transition temperatures of materials and the corresponding transition enthalpies. The optical textures were observed through a polarising microscope (Nikon optiphot-2-pol and Eclipse LV-100POL) equipped with a hot- and cold-stage HCS302, with STC200 temperature controller configured for HCS302 and Instec HS-ii hot stage from Instec Inc., USA. The textures were recorded using Nikon NIS elements attached with the polarising microscope.

3. Results and discussion

3.1. Mesomorphism

The unsymmetrical dimesogens **1-Bu** (can also be abbreviated as KI-4(OH) as in reference 40, 45), **1-F** and **1-Cl** were obtained by condensing *N*-[4-(5-cholesteryloxycarbonyl)-butyloxy)-salicylaldehyde and 4-substituted anilines. The introduction of ortho hydroxyl group in benzylidene moiety not only enhances the stability of the imines through intramolecular H-bonding to overcome the hydrolytic instability of the molecules towards moisture but also enhances the transverse dipole moment. Hence, the salicylidene aniline core present in these compounds promotes thermal stability which is confirmed by FTIR. In calamitic ferroelectric liquid crystals derived from achiral molecules, the resorcylidene aniline core actually found to be rather superior to the benzylidene aniline core with respect to mesogenicity and is more stable towards hydrolysis [46–50].

The salicylaldehyde derivative **3** for the synthesis of our target material **1-Bu**, **1-F** and **1-Cl** was obtained starting from cholesterol ω-bromopentanoate **2** which had been prepared by the esterification reaction of cholesterol **1** with 5-bromopentanoyl chloride in dichloromethane at room temperature in the presence of triethylamine as base. The synthetic details are furnished in the experimental section as detailed in Scheme 1. The molecular structures of intermediates and unsymmetrical dimesogens were authenticated by spectroscopic analysis. The phase transition temperatures and mesomorphic properties of the dimesogens **1-Bu**, **1-F** and **1-Cl** were examined by DSC and polarising optical microscopy (POM). All the compounds exhibit two mesophase transitions in heating and as well as cooling cycles as evidenced from DSC experiments during second heating and cooling cycles at 5°C/min and are in agreement with optically measured temperatures. All the

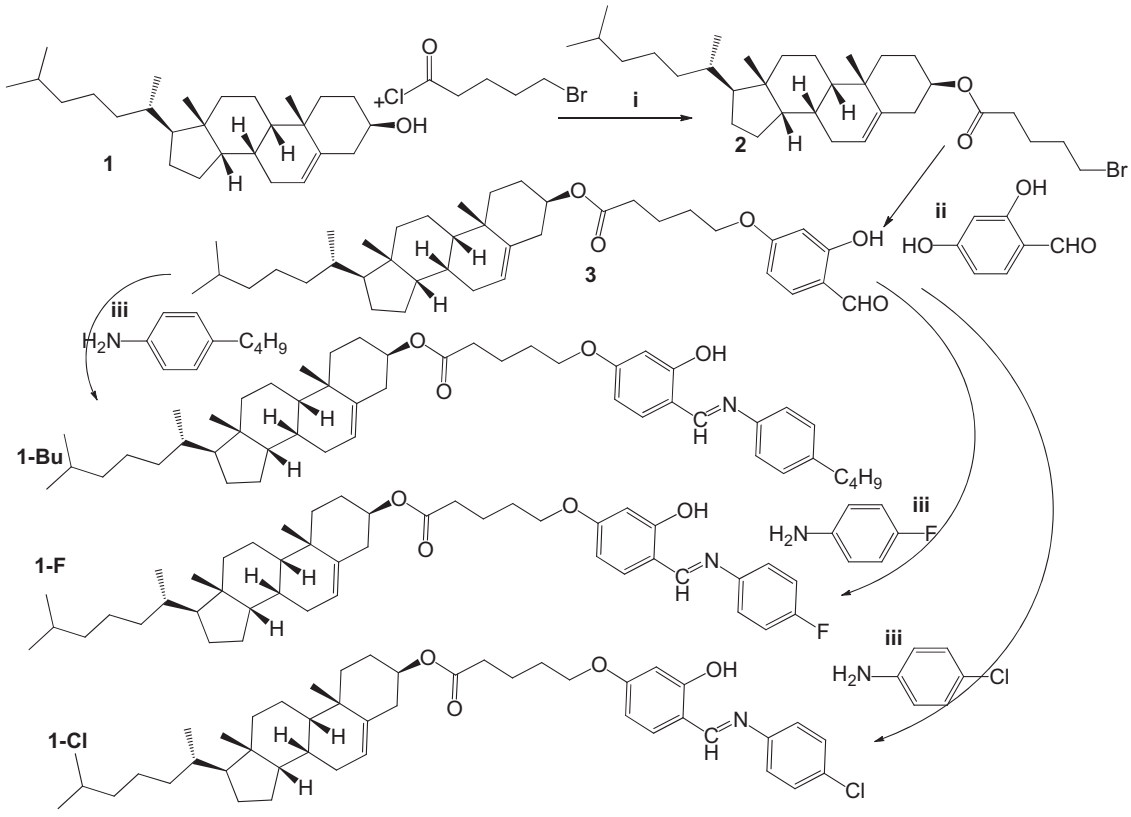

Scheme 1. Procedure for the preparation of compounds **1-Bu**, **1-F** and **1-Cl:** (i) DCM, TEA, RT, stirring 24 h; (ii) $KHCO_3$, acetone, KI, reflux 18 h; (iii) EtOH, AcOH, reflux 4 h.

phase transitions are enantiotropic in nature. The crystal to mesophase transition is associated with large enthalpy change, whereas the other phase transition exhibits small enthalpy and entropy changes. Transition enthalpies were obtained from the DSC traces. The phase transformations at BPIII-cubic BP (cubic BP: BPI or BPII [24–26]-N*-TGB/SmC* phases were observed in optical textures under POM without a signature in DSC spectra. Optical observations were made with untreated clean glass plates and cover slips or commercial cells treated for homogeneous or homeotropic alignments. The results are presented in Table 1.

Figures 1–3 illustrate the typical POM textures exhibited by pure compounds (**1-Bu**, **1-F** and **1-Cl**). Compound **1-Bu** exhibited only fan-shaped highly twisted texture resembling the N* phase (Figure 1). However, the replacement of methyl moiety by a polar fluoro substituent the mesomorphic behaviour had changed to SmC*-N*-cubic BP-BPIII phase variant. For chloro substituent, the phase variant was TGBA-N*-cubic BP-BPIII. On slow cooling (0.01°C/min) of **1-F**, the isotropic liquid changed to a foggy blue coloured phase (Figure 2a) with fluidity without the appearance of platelets resembling the characteristic textures observed for BPIII phase. BPIII is identified by the grazed platelet texture with a thermal range of ~0.6°C. Further cooling displayed a mosaic of colours and different coloured platelets within the mosaic which correspond to randomly oriented domains of crystalline BP orderingm suggesting the phase as cubic BP. On further cooling, the texture transformed into focal conic texture of N* phase with the absence of fingerprint striated texture. The focal conic texture is a signature of highly screwed chiral nematic liquid crystal with short helical pitch of nano-order. The distance between the finger print striae in this system is too small to be detected in polarising microscope with a resolution limit of ca. 1 μm. On further cooling a phase transition occurred at 94.5°C, showing the chiral lines running across the tiny focal conic pattern a diagnostic feature for the SmC* phase which continued till 45.0°C.

The observation of two different types of optical textures, namely helical texture characteristic of cholesteric organisation and CC domain texture with radial streaks and broken shape can be considered as the signature of the TGB phase in the compound **1-Cl**. The optical textures characteristic of BPIII and cubic BP are also exhibited by **1-Cl**. Further, **1-Cl**

Table 1. Phase transition temperatures (°C) of the compounds **1-Bu**, **1-F** and **1-Cl** recorded for second heating (first row) and second cooling (second row) cycles at 5°C/min from DSC and confirmed by polarised optical microscopy. The enthalpies (ΔH in kJ/mol) are presented in parentheses.

1-Bu	Cr			113.1 (7.31)	N*					161.3 (0.56)	I
	Cr			73.3 (7.46)	N*					160.9 (0.64)	I
1-F	Cr			129.6 (38.1)	N*					159.8°C (0.57)	I
	Cr	45°C	TGB	94.5°C (4.90)	N*	158.0°C	Cubic BP	158.6°C	BPIII	159.1°C (0.63)	I
1-Cl	Cr			115.5 (31.6)	N*					177.9°C (0.55)	I
	Cr	80.2°C	TGB*	74.1°C† (22.6)	N*	175.9	Cubic BP	176.5	BPIII	177.3°C (0.74)	I

Note: DSC runs are carried out at a rate of 5°C/minute in the second heating and cooling cycles only. Values in parentheses represent enthalpy in kJ/mol. All the transitions are not detected by DSC. The observed transition temperatures in POM studies in cooling cycle are recorded.
†Monotropic transition observed by POM studies.

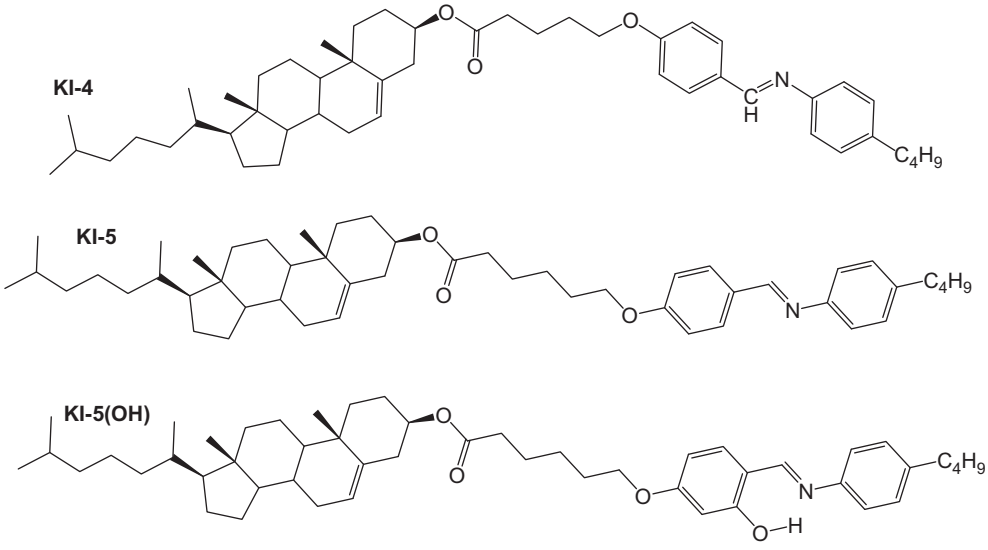

KI-4: Cr 85 SmC* 134 SmC* 141 TGB 142 N* 153.8 BPI 154.8 BPII 155.6 I [40].
KI-5(OH): Cr 130.1 SmA 174 (TGB transient) N* 203 I [45,53].
KI-5: Cr 85 SmAinc 144.5 SmC* 149 SmAinc 151.5 SmC* 165 TGB 168 N* 191 BP 192 I [39,40,] [SmAinc = incommensurate SmA].
KI-5: Cr 85 $S_{\check{C}}$ 97 S_{q3} 141 S_{ic} 146 Sm_{C^*LT} 152 Sm_{C^*HT} 164 TGB 168 N* 192 I [41].
$S_{\check{C}}$ = ribbon phase and closely resemble real S_{ic}, S_{ic} = incommensurate fluid smectic phase, S_{q3} is a two dimensional modulated smectic phase and exhibits two incommensurate lengths reflecting long range layer structure (q3) and the other reflecting short range order resulting in incommensurate fluctuations.

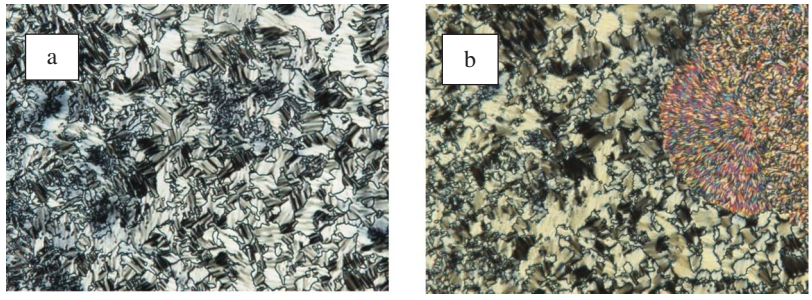

Figure 1. Optical polarising microscope photographs of **1-Bu**: (a) at 140°C in N* phase; (b) during phase transition at 50°C.

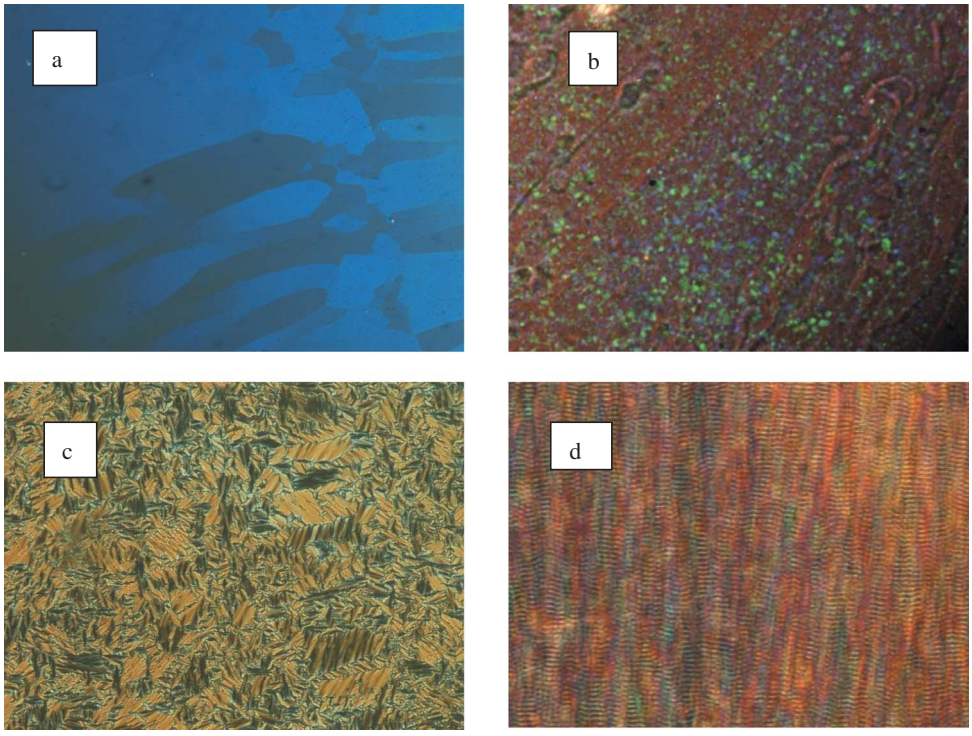

Figure 2. Optical polarising microscope photographs of **1-F**: (a) grazed platelet texture at 158.8°C of BPIII phase; (b) texture at 158.2°C of cubic BP phase; (c) highly twisted texture with fan-like appearance without any striae of the N* phase at 140.0°C; (d) chiral lines across the tiny focal-conic texture characteristic of SmC* phase below 94.0°C till 45°C.

also exhibited planar fingerprint texture of the N* phase, followed by sudden appearance of focal conic texture with helical axes distributed in all directions [51] as well as cylindrical or marginally cone-like (CC) domain texture [52] with radial streaks inside domains at low temperature and broken shape of the TGBA phase in cooling cycle. The observed CC domain textures may be seen as classical distinct focal conics or as developable domain texture confirm the TGBA phase [52].

The shortening of the central spacer to four methylene units promoted the appearance of twisted nematic phases in lieu of smectic polymorphism and disappearance of in-commensurate smectic phases [40]. The butyl homologue with benzylidene linkage (without the ortho hydroxyl group) **KI-4** (Table 1) exhibited two BPs over a temperature range of 1.8°C, in addition to TGB phase (1°C) and SmC* phases (56°C). When the central spacer is increased to five methylene units, the benzylidene homologue **KI-5** exhibited almost similar phase sequence. However, the salicylidene homologue **KI-5(OH)** exhibited N* and SmA phases with the occurrence of transient TGB phase and extinction of BP [45,53]. In the present work with the four methylene spacer, the salicylidene homologue **1-Bu** (equivalent terminology **KI-4(OH)**) exhibited only N* phase, whereas the introduction of polar substituent replacing the butyl moiety promoted the blue and TGB phases. The TGB phase consists of a helical stack of blocks of smectic liquid crystal separated by grain boundaries made up of an array of screw dislocations. In the Schiff base homologous series, it is reported that the smectic packing depends on the terminal substituent. Further, the unusual mesogenic moiety constituted by cholesteryl part the non-aromatic nature connected with its planar shape and its strong activity to interact favourably with the aliphatic chains probably allows a peculiar arrangement which supports the coexistence of varying periodicities of incommensurate fluid smectic phases.

In unsubstituted cholesteryl-4-*n*-alkoxybenzoates, the N*AC* phase variant is reported [54]. Further, the compounds, cholesteryl-2-fluoro-4-*n*-alkoxybenzoates, possessing strong lateral dipole moment exhibited enantiotropic BP, N*, TGB and smectic C* phases [55]. Thus, the occurrence of TGB phase has been attributed to the lateral dipole moment, since this substituent increases the transverse polarity of the system and stabilises titled molecular arrangement in smectic phase. It should be pointed out that the occurrence of TGB phase also depends on the length of alkoxy chain [56–62]. However, in cholesteryl-4-polyfluoroalkoxy-3-nitrobenzoate, possessing strong lateral dipole moment and rigid

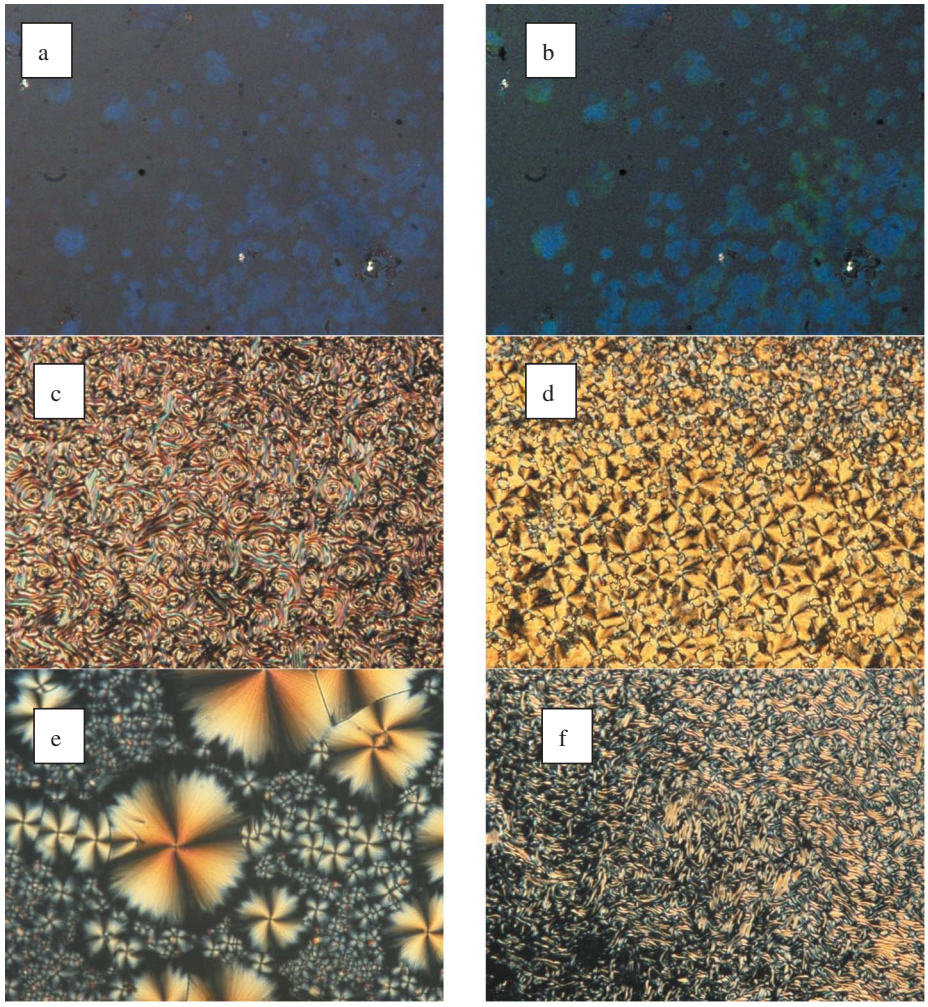

Figure 3. Optical polarising microscope photographs of **1-Cl**: (a) Foggy platelet texture at 177.1°C of BPIII phase; (b) texture at 176.1°C of cubic BP phase; (c) planar fingerprint texture of N* phase at 74.1°C; (d) **TGBA** phase with focal conic texture just below the transition to TGB phase at 74°C; (e) cylindrical or marginally cone-like (CC) domain textures with radial streaks and broken shape observed at $T = 40$°C of TGB phase. In the centre of the photograph one can observe that the 'two eyes' are very close to each other; (f) oily streak texture at room temperature.

perfluoroalkyl end chain, only N* and/or SmA phases are reported [63]. The unsubstituted analogues, cholesteryl-4-polyfluoroalkoxybenzoates, exhibited SmA and SmE phases [63–66].

3.1.1. Influence of polar fluoro substituent

The substitution of hydrogen by fluorine has become a widespread principle in drug design, materials chemistry and the molecular design of liquid crystals. Fluoro substituents have been successfully and usefully incorporated into liquid crystal molecules because of the combination of small size and high polarity [67–69]. The fluoro substituent in organic compounds is interesting because of the combination of polar and steric effects, and the strength of the C–F bond contributes to the stability of fluoro-substituted compounds. The highest electro-negativity of fluorine among all the elements (3.98) is responsible for a large polarisation of the C–F bond and hence as a substituent confers a large dipole moment on the C–F bond. In an aliphatic or alicyclic environment, the dipole moment is relatively large, for example, 1.85 D in fluoromethane, but in an aromatic environment, the mesomeric effect causes a reduction in electron density of aromatic system and hence dipole moment, for example, 1.50 D for fluorobenzene. The large polarisation of the C–F bond exhibits strong influence on the intermolecular dispersion interactions. It reflects in the induction of strong local dipole moments, electron density of the phenyl ring system and influences the π–π stacking of phenyl rings, π–H–C electrostatic interactions between phenyl rings, polarisation and polarisability of the molecular conjugated systems.

The relatively small size of a fluoro substituent does not unduly alter the molecular structure and helps to maintain the existing liquid crystalline nature of the compound. The fluoro substituent is the smallest (1.47Å), after hydrogen (1.2Å), of all possible substituents, and like hydrogen it is monoatomic. Although a fluoro substituent obviously causes a steric effect, the size influence is not too drastic, which enables it to be incorporated into parent molecules for beneficial modification of functional properties. Lateral substituents, particularly fluoro, are frequently employed in liquid crystal molecular structures to modify melting point, mesomorphic transition temperatures, phase morphology and the physical properties such as dielectric properties, viscosity of liquid crystals for their possible applications.

Hence, the pronounced bent molecular conformation of the constituent compounds, subtle changes in the substitution pattern, the length of the spacer and nature of end substituents have strong influence on the occurrence of BPs as well as different phase variants. The biaxial shape of the molecule due to bent molecular conformations augmented by molecular interactions may have promoted the observation of BPIII in these polar compounds.

3.2. Theoretical calculation using DFT method on cholesterol derivatives

DFT study has been performed to give more insight into the molecular conformation, electrostatic potential distribution and molecular polarisability of the cholesterol derivatives **1-Bu**, **1-F** and **1-Cl** (Figure 4a–c). Full geometry optimisations have been carried out without imposing any constraint using Gaussian 09 program package [70]. Spin-restricted DFT calculations were carried out in the framework of the generalised gradient approximation (GGA) using Becke3–Lee–Yang–Parr hybrid functional (B3LYP) exchange–correlation functional and the 6-31G (d, p) basis set [71,72]. We have used the B3LYP functional with the standard basis set 6-31 G due to its successful application for larger organic molecules as well as hydrogen bond systems in past [73–75].

An accurate HOMO and LUMO description, namely atomic orbital composition, absolute energy and relative energy gap, provides the important information related to photo-physical properties which helps for the design of new molecules and their tuning of distinct desired properties of the compounds. The HOMO and LUMO energies are calculated and presented in Table 2. The 3D iso-surface plots of the highest occupied molecular orbital (HOMO) and lowest unoccupied molecular orbital (LUMO) of the compounds are shown in Figure 5a–f. The HOMO–LUMO energy separation can be used as a measure of kinetic stability of the molecule and could indicate the reactivity pattern [76,77]. A large HOMO–LUMO gap implies a high kinetic stability and low chemical reactivity, because it is energetically unfavourable to add electrons to a high-lying LUMO or to extract electrons from a low-lying HOMO [77]. The HOMO–LUMO energy gaps for **1-Bu**, **1-F** and **1-Cl** are found to be 4.08, 4.09 and 4.05 eV, respectively, and suggests that the compounds are fairly stable. Further, the electron density of the molecular orbitals, that is, HOMO and LUMO of all the compounds are mainly concentrated in the aromatic region of the molecules. Dipole moment for all the compounds has been calculated along the three Cartesian directions. Dipole moment along the molecular long axis, that is, *X*-axis is much larger than the dipole moment component

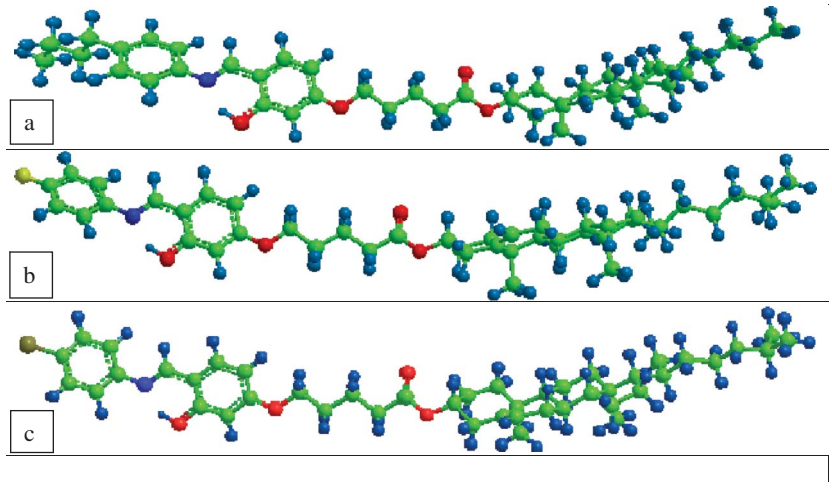

Figure 4. DFT optimised structrures of (a) **1-Bu**, (b) **1-F** and (c) **1-Cl**.

Table 2. DFT calculated HOMO, LUMO, energy gap, dipole moment components μ_x, μ_y, μ_z and modulus (μ) for compounds **1-Bu**, **1-F** and **1-Cl**.

Cholesterol derivatives	Energy (eV)			Dipole moment (μ in Debye)			
	HOMO	LUMO	ΔE (eV)	μ_x	μ_y	μ_z	μ_{total}
1-Bu	−5.50	−1.42	4.08	−2.5161	1.4156	−0.4638	2.9240
1-F	−5.63	−1.54	4.09	4.4498	0.7616	0.4907	4.5411
1-Cl	−5.72	−1.67	4.05	5.3712	0.5425	0.4667	5.4186

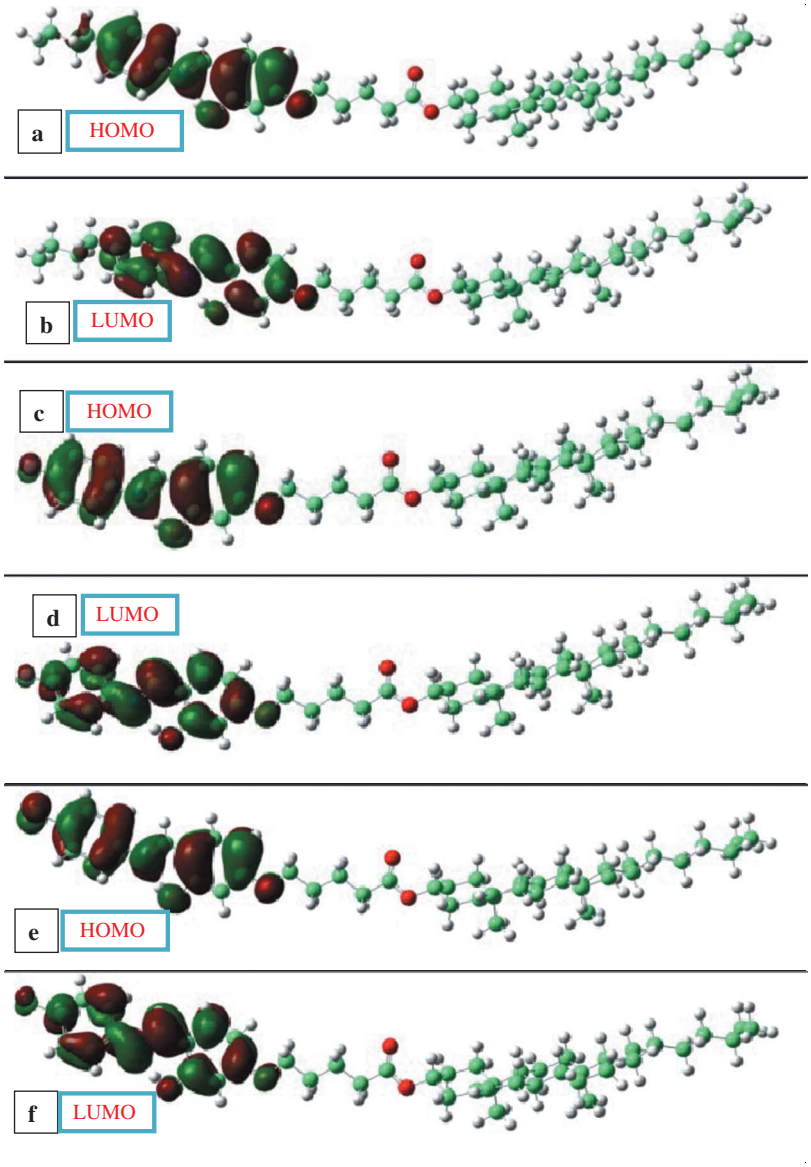

Figure 5. HOMO and LUMO surfaces of (a, b) **1-Bu**, (c, d) **1-F** and (e,f) **1-Cl**.

along the transverse axes. The dipole moments of the studied compounds are fairly larger than the dipole moment of cholesterol moiety reported earlier (1.59 D) [78]. Amongst the three cholesterol derivatives, polar compounds **1-Cl** and **1-F** have fairly larger dipole moment than **1-Bu**.

The electronic transitions in the UV-visible range of synthesised cholesterol derivatives (**1-Bu**,

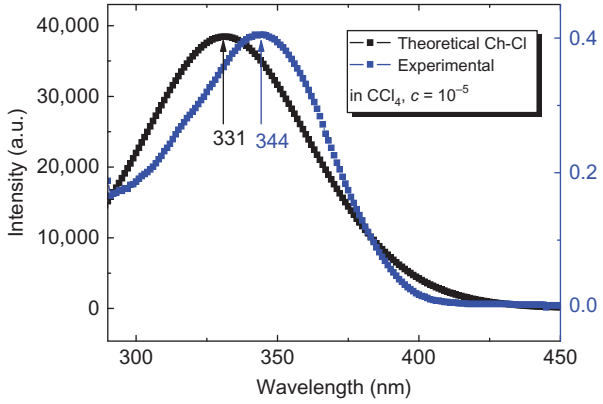

Figure 6. UV-visible absorption spectrum of **1-Cl** black line theoretical and blue line experimental.

1-F 1-Cl) have been studied. The UV-visible spectra of cholesterol derivatives have been simulated using the time-dependent density functional theory (TD-DFT) Becke3–Lee–Yang–Parr hybrid functional-6-31G (d, p) method. The experimental and theoretical absorbance as a function of wavelength is plotted in Figure 6. The experimental λ_{max} (331 nm) in solution, reflecting the π–π^* transition in the aromatic region, is in reasonable agreement with the theoretical value (344 nm) calculated in gaseous state.

Polarisabilities are crucial for an understanding of molecular properties in molecular optics and spectroscopy. Generally, molecular polarisability may strongly vary with molecular conformation, as has been shown, in particular for polypeptides and liquid crystals [79,80]. Electrostatic intermolecular interaction energy is related to polarisability, in particular for systems without a permanent dipole moment [81]. The polarisability α is largest along the molecular long X-axis (Table 3). The analysis revealed that the bend angle is approximately 163° (162–165°). However, due to the flexible nature of the central spacer, the calculated bending angle may not reflect the realistic conformation for each compound in a liquid crystalline phase. Hence, the asymmetry parameter (η) which is dependent on bend angle [68], as a possible indication is given by $\eta = [(\alpha_{YY} - \alpha_{ZZ})/(\alpha_{XX} - \alpha^{iso})]$, where α_{XX}, α_{YY} and α_{ZZ} are the principle components of the molecular polarisability tensor and α^{iso} is the isotropic molecular polarisability with $\alpha^{iso} = (\alpha_{XX} + \alpha_{YY} + \alpha_{ZZ})/3$). DFT calculated principal polarisability components (α_{XX}, α_{YY}, α_{ZZ}), isotropic polarisability component α^{iso}, polarisability anisotropy $\Delta\alpha = [\alpha_{XX} - (\alpha_{YY} + \alpha_{ZZ})/2]$ and asymmetry parameter, $\eta = [(\alpha_{YY} - \alpha_{ZZ})/(\alpha_{XX} - \alpha^{iso})]$, parameters relative to the molecular polarisability tensor, α, in the Cartesian reference frame are displayed in Figure 7. All polarisability components and the anisotropy parameter are expressed in Bohr^3 (with 1 Bohr = 0.52917Å). The asymmetry parameter for **1-Bu**, **1-F** and **1-Cl** are 0.18, 0.17 and 0.19, respectively, and is found to be rather small. For smaller values of η, mesomorphism not only stabilised but also thermal range is increased.

Nakata et al. reported [82] that an addition of a small amount of bent-core compound to the chiral nematic host can promote the emergence of BPs with wide thermal range, which had been recently confirmed by others [11,13,14,83] Further, these compounds with a bent angle of ~165° the BPs appeared in compounds with a polar group in the lateral direction.

Liquid crystals elements are involved in active matrix display (AMD) for which high voltage holding capability is needed for better contrast and flicker of display. The voltage holding ratio (VHR) is defined as the ratio of the voltages at a pixel at the end and the beginning of the frame time [84]. The VHR values can be correlated with electrostatic potentials [85]. The molecular shape of optimised **1-Bu** and **1-F** is sterically bulky. In addition, there are negative electrostatic potential (ESP) on the oxygen atoms (indicated by red contour) of the compound particularly on the ester carbonyl oxygen and phenolic oxygen atom as shown by colour variations, sky-blue represents a positive electrostatic potential (indicated by sky-blue contour) (Figure 8). The strong electrostatic centres favour strong interactions with positively charged cations. Hence, the absence of red centres in the majority

Table 3. DFT calculated principal polarisability components (α_{XX}, α_{YY}, α_{ZZ}), isotropic component $\alpha_{iso} = (\alpha_{XX,} + \alpha_{YY} + \alpha_{ZZ})/3$, polarisability anisotropy $\Delta\alpha = [\alpha_{XX} - (\alpha_{YY} + \alpha_{ZZ})/2]$ and asymmetry parameter $\eta_\alpha = (\alpha_{YY} - \alpha_{ZZ})/(\alpha_{XX,} - \alpha^{iso})]$, relative to the molecular polarisability tensor, α, and bend angle in the Cartesian reference frame presented in Figures 4 and 7.

Compound	α_{XX}	α_{YY}	α_{ZZ}	α^{iso}	$\Delta\alpha$	η_α	Bending angle (°)
1-Bu	927	455	390	590	505	0.19	162
1-F	839	411	355	535	456	0.18	165
1-Cl	881	417	359	552	493	0.17	164

Note: All principal polarisability components and the polarisability anisotropy parameter are expressed in Bohr^3 (Bohr = 0.52917Å).

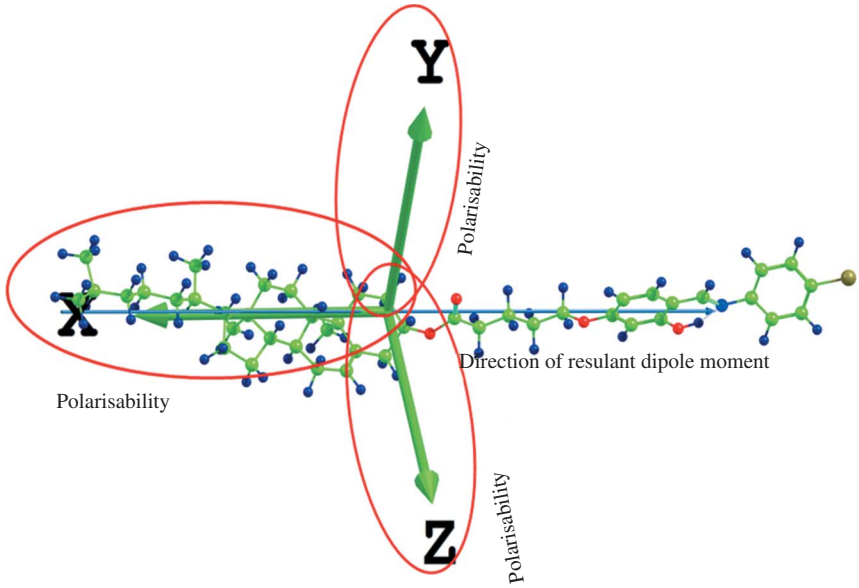

Figure 7. Distribution of static polarisability components in X, Y and Z directions and direction of resultant dipole moment of **1-Cl**.

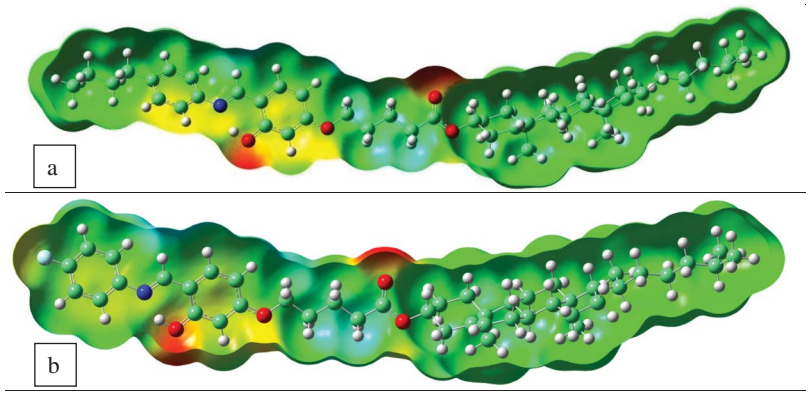

Figure 8. Isoelectron density surface with electrostatic potential of **1-Bu** and **1-F**. Red and sky-blue surfaces indicate negative and positive electrostatic potential, respectively.

surface area of the molecule denotes a relatively high VHR value for this compound. Hence, homogenous distribution of partial charges lowers the ability to form cationic complexes by local electrostatic interactions and correlates reasonably well with high VHR of material. From the total ESP surface, it is clear that electron density is almost homogeneously distributed along the synthesised **1-Bu** and **1-F** molecules which indicates the applicability of this type of molecules in mixtures and also gives an indication in the design of molecules.

4. Conclusion

The dimesogens consisting of promesogenic cholesteryl moiety and Schiff base with an end alkyl or polar fluoro or chloro groups linked through an even parity alkylene spacer are synthesised and characterised. All the compounds found to possess bend shape with a bent angle ~160° from the DFT study. The bent angle may not exactly reflect actual bent angle in a condensed phase due to the flexible nature of the spacer but still it can be approximated as a guide to visualise the shape of the molecules. In general, in unsymmetrical dimers, trimers [86] and tetramers [87] intercalated smectic phases have been reported and the driving force for the formation of such intercalated smectic phases is derived from specific interactions, namely the nature of the linking group between the spacer and mesogenic units, interactions between the incompatible molecular subunits in the molecule, and so on. In the present work, we did not observe such intercalated smectic phases, instead frustrated phases are observed. The

polar fluoro and chloro compounds found to exhibit frustrated BPs with a small thermal range. The fluoro homologue exhibited SmC^* phase while chloro homologue exhibited TGB phase for a reasonably long thermal range. Further work is in progress to investigate the bent shape influence on enhancement of BP thermal range in mixtures. DFT study indicated the presence of homogeneously distributed electron density and negligible negative electrostatic potential in these molecules.

5. Synthesis

5.1. Cholesteryl 5-bromopentanoate, 2

5-Bromovaleric acid (1.81 g, 10 mmol) was treated with $SOCl_2$ (3 ml) to get the corresponding acid chloride. Ester derivative was prepared by the esterification reaction of cholesterol (3.86 g, 10 mmol) with 5-bromovaleric acid chloride (1.99 g, 10 mmol) in tetrahydrofuran at room temperature in the presence of few drops of pyridine as base. The product was then purified by column chromatography using silica gel (60 mesh) with hexane as eluent. The product was obtained as white solid. Yield = 3.95 g (72.4%). IR (KBr, cm^{-1}): ν_{max}: 2956 and 2850 (C–H stretching), 1732 (C=O stretching), 1598 and 1566 (C=C stretching), 1250 and 1172 (C–O stretching).

5.2. Cholesteryl 5-(3-hydroxy-4-formylphenoxy) pentanoate, 3

A mixture of cholesteryl 5-bromopentanoate (2.2 g, 4 mmol), 2,4-dihydroxybenzaldehyde (0.55 g, 4 mmol), potassium hydrogen carbonate (2.0 g, 20 mmol) and KI (catalytic amount) were dissolved in dry acetone and then the mixture was refluxed for 24 h. It was then filtered hot to remove the insoluble solid. The solvent was evaporated to get the solid. Then the solid was purified by column chromatography using silica gel (60–120 mesh) with hexane:chloroform (9:1) as eluent. The product was recrystallised from a mixture of DCM–ethanol and pure product was obtained as off-white solid. Yield = 1.4 g (60%).

Elemental analysis calculated for $C_{39}H_{58}O_5$, C 77.19, H 9.63; found C 77.01, H 9.51%.

General synthetic procedure for the preparation of dimesogenic compounds **1-Bu**, **1-F** and **1-Cl**.

A mixture of cholesteryl 5-(3-hydroxy-4-formylphenoxy)pentanoate **3** (0.6 g, 1 mmol) was dissolved in absolute ethanol and heated to reflux along with few drops of glacial acetic acid. To this solution, ethanolic solution of 4-n-butylaniline (0.15 g, 1 mmol) (or 4-fluoroaniline/4-chloroaniline 1 mmol) was added drop wise and further refluxed for 2 h. The yellow precipitate was filtered, dried and recrystallised several times from ethanol to yield pure product. All the products were obtained in quantitative yield.

5.3. N-[4-(5-cholesteryloxycarbonyl)-butyloxy)-salicylidene]-4-n-butylaniline, 1-Bu

White solid; FTIR (KBr, cm^{-1}): ν_{max}: 3429 (O–H, H bonding), 2951 and 2868 (C–H stretching), 1732 (ester C=O stretching), 1618 (C=N stretching), 1598 and 1566 (Ar C=C stretching), 1250 and 1172 (ester C–O stretching), 1159 (ester C–O–C stretching. Elemental analysis: Calculated for $C_{49}H_{71}NO_4$, C 79.74, H 9.70; found C 79.57, H 9.61%.

^{1}H NMR (500 MHz, $CDCl_3$): δ13.92, (s, 1H, OH), 8.52 (s, 1H, CH=N), 7.24 (d, J = 6.9 Hz 1H, Ar), 7.20 (d, J = 6.9 Hz, 4H, ArH), 6.47 (d, J = 2.4 Hz, 1H, Ar), 6.45 (dd, J = 2.3, 7.6 Hz, 1H, Ar), 5.37 (br, 1H, olefinic), 4.62 (m, 1H, OCH), 4.01 (t, J = 5.7, 2H, OCH_2), 2.62 (t, J = 7.65, 2H, $ArCH_2$), 2.37 (m, 4H, 2 × allylic methylene), 2.02–0.90 (m, 43H, 6 × CH, 14 × CH_2, 3 × CH_3), 0.86 (d, J = 2.30, 3H, CH_3), 0.85 (d, J = 2.30, 3H, CH_3) and 0.67 (s, 3H, CH_3).

5.4. N-[4-(5-cholesteryloxycarbonyl)-butyloxy)-salicylidene]-4-fluoroaniline, 1-F

Yield: 70%, white solid; FTIR (KBr, cm^{-1}): ν_{max}: 3427, 2956 and 2850 (C–H stretching), 1728 (C=O stretching), 1614 (C=N stretching), 1598 and 1566 (C=C stretching), 1250 and 1172 (C–O stretching). Elemental analysis: Calculated for $C_{45}H_{62}FNO_4$, C 77.21, H 8.93 Found C 77.03, H 8.74%

^{1}H NMR (500 MHz, $CDCl_3$): δ13.60, (s, 1H, OH), 8.49 (s, 1H, CH=N), 7.28–7.11 (m, 5H, Ar), 6.49 (d, J = 7.6 Hz, 1H, Ar), 6.49 (d, J = 2.4 Hz, 1H, Ar), 5.37 (br, 1H, olefinic), 4.64 (b, 1H, OCH), 4.02 (t, 2H, OCH_2), 2.37 (m, 4H, 2 × allylic methylene), 2.02–0.90 (m, 36H, 6 × CH, 12 × CH_2 2 × CH_3), 0.87 (d, J = 2.30, 6H, 2 × CH_3) and 0.67 (s, 3H, CH_3).

5.5. N-[4-(5-cholesteryloxycarbonyl)-butyloxy)-salicylidene]-4-chloroaniline, 1-Cl

Yield: 72%, white solid; FTIR (KBr, cm^{-1}): ν_{max}: 3427, 2956 and 2850 (C–H stretching), 1728 (C=O stretching), 1633 (C=N stretching), 1598 and 1566 (C=C stretching), 1250 and 1172 (C–O stretching). Elemental analysis: Calculated for $C_{45}H_{62}ClNO_4$, C 75.44, H 8.72 Found C 75.34, H 8.65%.

^{1}H NMR (500 MHz, $CDCl_3$): δ13.5, (s, 1H, OH), 8.51 (s, 1H, CH = N), 7.37 (d, J = 6.4 Hz 1H, Ar), 7.28 (d, J = 5.6 Hz, 2H, Ar), 7.21 (d, J = 6.8 Hz, 2H, ArH), 6.50 (dd, J = 2.8, 7.6 Hz, 1H, Ar), 6.49 (d, J = 2.4 Hz, 1H, Ar), 5.38 (brd, 1H, olefinic), 4.62 (m, 1H, OCH),

4.03 (t, $J = 6.0$ Hz, 2H, OCH_2), 2.38-2.32 (m, 4H, 2 × allylic methylene), 2.02–0.90 (m, 36H, 6 × CH, 12 × CH_2, 2 × CH_3), 0.86 (d, $J = 2.30$, 3H, CH_3), 0.85 (d, $J = 2.30$, 3H, CH_3) and 0.67 (s, 3H, CH_3).

Acknowledgement

Financial assistance provided by DST, DAE, NRBD and UGC, India, are gratefully acknowledged.

References

[1] Reinitzer F. Beitrage zur kenntniss des cholesterins. Monatsh Chem. 1888;9:421–441.
[2] Kitzerow H. Twist grain boundary phases. In: Kitzerow HS, Bahr C, editors. Chirality in liquid crystals. New York: Springer-Verlag; 2001. p. 296–354.
[3] Kishikawa K, Itoh H, Akiyama S, Kobayashi T, Kohmoto S. Stabilization of the blue phases of simple rodlike monoester compounds by addition of their achiral homologues. J Mater Chem. 2012;22:8484–8491.
[4] Yoshizawa A, Sato M, Rokunohe J. A blue phase observed for a novel chiral compound possessing molecular biaxiality. J Mater Chem. 2005;15:3285–3290.
[5] Kikuchi H. Liquid crystalline blue phases. Struct Bond. 2008;128:99–117.
[6] Kikuchi H, Yokota M, Hisakado Y, Yang H, Kajiyama T. Polymer-stabilized liquid crystal blue phases. Nat Mater. 2002;1:64–68.
[7] Kitzerow HS. Blue phases: prior art, potential polar effects, challenges. Ferroelectrics. 2010;395:66–85.
[8] Coles HJ, Pivnenko MN. Liquid crystal blue phases with a wide temperature range. Nature. 2005;436:997–1000.
[9] Yamamoto J, Nishiyama I, Inoue M, Yokoyama H. Optical isotropy and iridescence in a smectic blue phase. Nature. 2005;437:525–528.
[10] Crooker PP. Blue phases. In: Kitzerow HS, Bahr C, editors. Chirality in liquid crystals. New York: Springer; 2001. p. 186–222.
[11] Kitzerow HS. Blue phases at work. Chem Phys Chem. 2006;7:63–66.
[12] Meiboom S, Sethna JP, Anderson PW, Brinkman WF. Theory of the blue phase of cholesteric liquid crystals. Phys Rev Lett. 1981;46:1216–1219.
[13] Yelamaggad CV, Bonde NL, Achalkumar AS, Rao DSS, Prasad SK, Prajapati AK. Frustrated liquid crystals: synthesis and mesomorphic behavior of unsymmetrical dimers possessing chiral and fluorescent entities. Chem Mater. 2007;19:2463–2472.
[14] Wright DC, Mermin ND. Crystalline liquids: the blue phase. Rev Mod Phys. 1989;61:385–432.
[15] Dierking I, Blenkhorn W, Credland E, Drake W, Kociuruba R, Kayser B, Michael T. Stabilising liquid crystalline blue phases. Soft Matter. 2012;8:4355–4362.
[16] Hur ST, Gim MG, Yoo HJ, Choi SW, Takezoe H. Investigation for correlation between elastic constant and thermal stability of liquid crystalline blue phase I. Soft Matter. 2011;7:8800–8803.
[17] Zheng Z, Shen D, Huang P. Wide blue phase range of chiral nematic liquid crystal doped with bent-shaped molecules. New J Phys. 2010;12:113018 (10pp.).
[18] Goodby JW, Waugh MA, Stein SM, Chin E, Pindak R, Patel JS. A new molecular ordering in helical liquid crystals. J Am Chem Soc. 1989;111:8119–8125.
[19] Goodby JW, Waugh MA, Stein SM, Chin E, Pindak R, Patel JS. Characterization of a new helical smectic liquid crystal. Nature. 1989;337:449–452.
[20] Goodby JW, Slaney AJ, Booth CJ, Nishiyama I, Vuijk JD, Styring P,Toyne KJ. Chirality and frustration in ordered fluids. Mol Cryst Liq Cryst. 1994;243:231–298.
[21] Goodby JW. Twist grain boundary and frustrated liquid crystal phases. Curr Opin Coll Inter Sci. 2002;7:326–332.
[22] Goodby JW. Chirality in liquid crystals. J Mater Chem. 1991;1:307–318.
[23] Taushanoff S, Le KV, Williams J, Twieg RJ, Sadashiva BK, Takezoe H, Jakli A. Stable amorphous blue phase of bent-core nematic liquid crystals doped with a chiral material. J Mater Chem. 2010;20:5893–5898.
[24] Yoshizawa A, Kogawa Y, Kobayashi K,Takanishi Y, Yamamoto J. A binaphthyl derivative with a wide temperature range of a blue phase. J Mater Chem. 2009;19:5759–5764.
[25] Kogawa Y, Hirose T, Yoshizawa A. Biphenyl derivative stabilizing blue phases. J Mater Chem. 2011;21:19132–19137.
[26] Tanaka M, Yoshizawa A. U-shaped oligomers with a molecular biaxiality stabilizing blue phases. J Mater Chem. 2013. doi:10.1039/C2TC00105E.
[27] Lee M, Hur ST, Higuchi H, Song K, Choi SW, Kikuchi H. Liquid crystalline blue phase I observed for a bent-core molecule and its electro-optical performance. J Mater Chem. 2010;20:5813–5816.
[28] He W, Pan G, Yang Z, Zhao D, Niu G, Huang W, Yuan X, Guo J, Cao H, Yang H. Wide blue phase range in a hydrogen-bonded self-assembled complex of chiral fluoro-substituted benzoic acid and pyridine derivative. Adv Mater. 2009;21:2050–2053.
[29] Imrie CT, Henderson PA. Liquid crystal oligomers: going beyond dimers. Liq Cryst. 2009;36:755–777.
[30] Imrie CT, Henderson PA. Liquid crystal dimers and higher oligomers: between monomers and polymers. Chem Soc Rev. 2007;36:2096–2124.
[31] Majumdar KC, Ghosh T, Rao DSS, Prasad SK. Unsymmetrical cholesterol and benzoxazole-based liquid crystalline dimers: synthesis and characterization. Liq Cryst. 2011;38:1269–1277.
[32] Majumdar KC, Shyam PK, Rao DSS, Prasad SK. Oxadiazole-based unsymmetrical chiral liquid crystal dimers: synthesis and mesomorphic properties. Liq Cryst. 2012;39:1358–1367.
[33] Chan T, Lu Z, Yam WS, Yeap GY, Imrie CT. Non-symmetric liquid crystal dimers containing an isoflavone moiety. Liq Cryst. 2012;39:393–402.
[34] Yeap GY, Chan TN, Yam WS, Madrak K, Pociecha D, Gorecka E. Non-symmetric chiral isoflavone dimers: synthesis, characterisation and mesomorphic behaviour. Liq Cryst. 2012;39:1041–1047.
[35] Donaldson T, Staesche H, Lu ZB, Henderson PA, Achard MF, Imrie CT. Symmetric and non-symmetric chiral liquid crystal dimers. Liq Cryst. 2010;37:1097–1110.
[36] Lee HC, Lu Z, Henderson PA, Achard MF, Mahmood WAK, Yeap GY, Imrie CT. Cholesteryl-based liquid crystal dimers containing a sulfur-sulfur link in the flexible spacer. Liq Cryst. 2012;39:259–268.

[37] Yelamaggad CV, Shashikala IS, Liao G, Rao DSS, Prasad SK, Li Q, Jakli A. Blue phase, smectic fluids, and unprecedented sequences in liquid crystal dimers. Chem Mater. 2006;18:6100–6102.
[38] Yelamaggad CV, Mathews M, Hiremath US, Rao DSS, Prasad SK. Cholesterol-based non-symmetric liquid crystal dimers: an overview. J Mater Chem. 2008;18:2927–2949.
[39] Hardouin F, Achard FM, Jin JI, Shin JW, Yun YK. Novel sequence with incommensurate SA phases in a new dimesogenic liquid crystal. J Phys II. 1994;4:627–643.
[40] Hardouin F, Achard MF, Jin JI, Yun YK. From incommensurability to commensurability in smectic phases for a series of dimesogenic liquid crystals. J Phys II. 1995;5:927–935.
[41] Hardouin F, Achard MF, Jin JI, Yun YK, Chung SJ. Competition in low ordered smectics between incommensurate phases Sic and two-dimensional modulated ones for dimesogenic compounds. Eur Phys JB. 1998;1:47–56.
[42] Lee JW, Park Y, Jin J, Achard MF, Hardouin F. Comparison of the liquid crystalline properties of dimesogenic compounds bearing alkoxy and perfluoroalkoxy tails. J Mater Chem. 2003;13:1367–1372.
[43] Yelamaggad CV, Prabhu R, Shanker G, Bruce DW. Optically active, mesogenic lanthanide complexes: design, synthesis and characterisation. Liq Cryst. 2009;36:247–255.
[44] Shanker G, Yelamaggad CV. A new class of low molar mass chiral metallomesogens: synthesis and characterization. J Mater Chem. 2011;21:15279–15287.
[45] Yelamaggad CV, Hiremath US, Rao DSS. Cholesterol-based dimesogenic bidentate ligands and their Cu(II) and Pd(II) metallomesogens. Liq Cryst. 2001;28:351–355.
[46] Ostrovskii BI, Rabinovich AZ, Sonin AS, Sorkin EL, Strukov BA, Taraskin SA. Ferroelctric behaviour of different classes of smectic liquid crystals. Ferroelectrics. 1980;24:309–312.
[47] Hallsby A, Nilsson M, Otterholm B. Synthesis of Schiff bases forming the first room temperature ferroelectric liquid crystal-the MORA series. Mol Cryst Liq Cryst. 1982;82:61–68.
[48] Otterholm B, Nilsson M, Lagerwall ST, Skarp K. Properties of some broad band chiral smectic C materials. Liq Cryst. 1987;2:757–768.
[49] Bustamante EAS, Yablonskii SV, Ostrovskii BI, Beresnev LA, Blinov LM, Haase W. Antiferroelectric behaviour of achiral mesogenic polymer mixtures. Liq Cryst. 1996;21:829–839.
[50] Blinov LM. Uniaxial and biaxial liquid crystal phases in colloidal dispersions of board-like particles. Liq Cryst. 1998;24:143–152.
[51] Cruz CD, Rouillin JC, Marcerou JP, Isaert N, Nguyen HT. Synthesis and mesomorphic properties of a new chiral series with anticlinic and TGB phases. Liq Cryst. 2001;28:125–137.
[52] Ribeiro AC, Nguyen HT, Galerne Y, Guillon D. Optical textures in TGBA mesophases. Liq Cryst. 2000;27:27–34.
[53] Yelamaggad CV, Hiremath US, Nagamani SA, Rao DSS, Prasad SK. Novel chiral dimesogenic bidentate ligands and their Cu(II) and Pd(II) metal complexes. Liq Cryst. 2003;30:681–690.
[54] Vill V, Thiem J. Ferroelektrische cholesterin derivate. Z Naturforsch. 1990;45a:1205–1210.
[55] Shubashree S, Sadashiva BK. Twist grain boundary smectic A phase in compounds derived from cholesterol. Curr Sci. 2003;85:1061–1065.
[56] Cha SW, Jin JI, Achard F, Hardouin MF. Anomalies of periodicity in TGB structures in new liquid crystal dimmers. Liq Cryst. 2002;29:755–763.
[57] Yelamaggad CV, Srikrishna A, Rao DSS, Prasad SK. Synthesis and characterization of some new dimesogenic compounds. Liq Cryst. 1999;26:1547–1554.
[58] Yelamaggad CVA. Novel Dirnesogen with a Cholesteric Phase of wide temperature range: synthesis and characterisation. Mol Cryst Liq Cryst. 1999;326:149–153.
[59] Yelamaggad CV, Nagamani SA, Rao DSS, Prasad SK, Hiremath US. Electroclinic effect in unsymmetrical dimeric liquid crystals composed of two non-identical chiral mesogenic entities. Mol Cryst Liq Cryst. 2001;363:1–17.
[60] Yelamaggad CV, Nagamani SA, Hiremath US, Rao DSS, Prasad SK. Unsymmetrical trimesogens exhibiting the undulated twist grain boundary(UTGBS*) mesophase. Liq Cryst. 2001;28:1581–1583.
[61] Yelamaggad CV, Hiremath US, Rao DSS, Prasad SK. A novel calamitic liquid crystalline oligomer composed of three non-identical mesogenic entities: synthesis and characterization. Chem Comm. 2000;57–58. doi:10.1039/A907974B.
[62] Yelamaggad CV, Nagamani SA, Hiremath US, Nair GG. Cholesterol-based dimeric liquid crystals: synthesis and mesomorphic behaviour. Liq Cryst. 2001;28:1009–1015.
[63] Wen J, Chen H, Shen Y. The first series of ferroelectric steroidal fluorinated liquid crystals. Liq Cryst. 1999;26:1833–1834.
[64] Wang K, Li H, Wen J. Synthesis and mesomorphic properties of cholesteryl p-polyfluoroalkoxy-m-nitrobenzoate. J Fluorine Chem. 2001;109:205–208.
[65] Qin C, Rong G, Wen J, Vajda A, Eber N, Synthesis and mesomorphic properties of cholesteryl *p*-2,2,3,3,4,4,5,5-octafluoropentoxybenzoate. Liq Cryst. 2004;31:1677–1679.
[66] Wang K, Shen Y, Yang Y, Wen J. Synthesis and mesomorphic properties of steroidal liquid crystals containing perflouoroalkoxycarbonylphenyl units. Liq Cryst. 2001;28:1579–1580.
[67] Smart BE. Characteristics of C–F systems. In: Banks RE, Smart BE, Tatlow JC, editors. Organofluorine chemistry principles and commercial applications. New York: Plenum Press. 1994; p. 57–88.
[68] Guittard F, Geribaldi S. Highly fluorinated molecular organised systems: strategy and concept. J Fluorine Chem. 2001;107:363–374.
[69] Guittard F, deGivenchy ET, Geribaldi S, Cambon A. Highly fluorinated thermotropic liquid crystals. J Fluorine Chem. 1999;100:85–96.
[70] Frisch MJ, Trucks GW, Schlegel HB, Scuseria GE, Robb MA, Cheeseman JR, Scalmani G, Barone V, Mennucci B, Petersson GA, Nakatsuji H, Caricato M, Li X, Hratchian HP, Izmaylov AF, Bloino J, Zheng G, Sonnenberg JL, Hada M, Ehara M, Toyota K, Fukuda R, Hasegawa J, Ishida M, Nakajima T, Honda Y, Kitao O, Nakai H, Vreven T, Montgomery JAJr, Peralta JE, Ogliaro F, Bearpark M, Heyd JJ,

Brothers E, Kudin KN, Staroverov VN, Kobayashi R, Normand J, Raghavachari K, Rendell A, Burant JC, Iyengar SS, Tomasi J, Cossi M, Rega N, Millam NJ, Klene M, Knox JE, Cross JB, Bakken V, Adamo C, Jaramillo J, Gomperts R, Stratmann RE, Yazyev O, Austin AJ, Cammi R, Pomelli C, Ochterski JW, Martin RL, Morokuma K, Zakrzewski VG, Voth GA, Salvador P, Dannenberg JJ, Dapprich S, Daniels AD, Farkas O, Foresman JB, Ortiz JV, Cioslowski J, Fox DJ. GAUSSIAN 09 (Revision B.01). Wallingford (CT): Gaussian, Inc.; 2010.

[71] Kim K, Jordan KD. Comparison of density functional and MP2 calculations on the water monomer and dimer. J Phys Chem. 1994;98:10089–10094.

[72] Stephens PJ, Devlin FJ, Chabalowski CF, Frisch MJ. Ab initio calculation of vibrational absorption and circular dichroism spectra using density functional force fields. J Phys Chem. 1994;98:11623–11627.

[73] Leach AR. Molecular modelling – principles and applications. 2nd ed. England: Pearson Education Limited; 2001.

[74] March NH. Electron density theory of atoms and molecules. London: Academic; 1992.

[75] Kryachko ES, Ludena EV, Energy density functional theory of many-electron system. Dordrecht: Kluwer; 1990.

[76] Kim KH, Han YK, Jung J. Basis set effects on relative energies and HOMO-LUMO energy gaps of fullerene C36. Theor Chem Acc. 2005;113:233–237.

[77] Aihara J. Reduced HOMO–LUMO gap as an index of kinetic stability for polycyclic aromatic hydrocarbons. J Phys Chem A. 1999;103:7487–7495.

[78] Osman O, Moawad H. Molecular spectroscopic analyses of cholesterol. J Appl Sci Res. 2010;6:1701–1704.

[79] Antoine R, Compagnon I, Rayane D, Broyer M, Dugourd P, Breaux G, Hagemeister FC, Pippen D, Hudgins RR, Jarrold MF. Electric susceptibility of unsolvated glycine-based peptides. J Am Chem Soc. 2002;124:6737–6741.

[80] Seltmann J, Marini A, Mennucci B, Dey S, Kumar S, Lehmann M. Nonsymmetric bent-core liquid crystals based on a 1,3,4-thiadiazole core unit and their nematic mesomorphism. Chem Mater. 2011;23: 2630–2636.

[81] Koch W, Holthausen MC. A chemist's guide to density functional theory. 2nd ed. Weinheim: Wiley-VCH Verlag GmbH; 2001.

[82] Nakata M, Takanishi Y, Watanabe J, Takezoe H. Blue phases induced by doping chiral nematic liquid crystals with nonchiral molecules. Phys Rev E. 2003;68:041710 (6pp.).

[83] Le KV, Aya S, Sasaki Y, Choi H, Araoka F, Ema K, Mieczkowski J, Jakli A, Ishikawa K, Takezoe H. Liquid crystalline amorphous blue phase and its large electrooptical Kerr effect. J Mater Chem. 2011;21:2855–2857.

[84] Schadt M. Field-effect liquid-crystal displays and liquid-crystal materials: key technologies of the 1990s. Displays. 1992;13:11–34.

[85] Lee SH, Bhattacharya SS, Jin HS, Jeong KU. Devices and materials for high-performance mobile liquid crystal displays. J Mater Chem. 2012;22:11893–11903.

[86] Donaldson T, Henderson PA, Achard MF, Imrie CT. Non-symmetric chiral liquid crystal trimers. Liq Cryst. 2011;38:1331–1339.

[87] Donaldson T, Henderson PA, Achard MF, Imrie CT. Chiral liquid crystal tetramers. J Mater Chem. 2011;21:10935–109341.